

# Iron Based Superconductors: Pnictides versus Chalcogenides

M.V. Sadovskii<sup>a,b</sup>, E.Z. Kuchinskii<sup>a</sup>, I.A. Nekrasov<sup>a</sup>

<sup>a</sup>*Institute for Electrophysics, Russian Academy of Sciences, Ural Branch, Amundsen str. 106, Ekaterinburg, 620016, Russia*

<sup>b</sup>*Institute for Metal Physics, Russian Academy of Sciences, Ural Branch, S. Kovalevskaya str. 18, Ekaterinburg, 620990, Russia*

## Abstract

We present a brief review of the present day situation with studies of high-temperature superconductivity in iron pnictides and chalcogenides. Recent discovery of superconductivity with  $T_c > 30$  K in  $A_x\text{Fe}_{2-x/2}\text{Se}_2$  ( $A=\text{K}, \text{Cs}, \text{Tl}$ ) represents the major new step in the development of new concepts in the physics of Fe - based high-temperature superconductors. We compare LDA and ARPES data on the band structure and Fermi surfaces of novel superconductors and those of the previously studied FeAs superconductors, especially isostructural 122 - superconductors like  $\text{BaFe}_2\text{As}_2$ . It appears that electronic structure of new superconductors is rather different from that of FeAs 122 - systems. In particular, no nesting properties of electron and hole - like Fermi surfaces is observed, casting doubts on most popular theoretical schemes of Cooper pairing for these systems. Doping of novel materials is extremely important as a number of topological transitions of Fermi surface near the  $\Gamma$  point in the Brillouin zone are observed for different doping levels. The discovery of Fe vacancies ordering and antiferromagnetic (AFM) ordering at pretty high temperatures ( $T_N > 500$  K), much exceeding superconducting  $T_c$  makes these systems unique antiferromagnetic superconductors with highest  $T_N$  observed up to now. This poses very difficult problems for theoretical understanding of superconductivity. We discuss the role of both vacancies and AFM ordering in transformations of band structure and Fermi surfaces, as well as their importance for superconductivity. In particular, we show that system remains metallic with unfolded Fermi surfaces quite similar to that in paramagnetic state. Superconducting transition temperature  $T_c$  of new superconductors is discussed within the general picture of superconductivity in multiple band systems. It is demonstrated that both in FeAs - superconductors and in new FeSe - systems the value of  $T_c$  correlates with the value of the total density of states (DOS) at the Fermi level.

## Key words:

Electronic structure, Superconductivity, Antiferromagnetism, Angle resolved photoemission spectroscopy

PACS: 74.25.Jb, 74.20.Fg, 75.59.Ee

## 1. Introduction

Discovery of iron based high-temperature superconductors [1] attracted a lot of scientific attention leading to a remarkable flow of experimental and theoretical works (for review see [2, 3]). The main classes of iron (pnictides and chalcogenides) based superconductors known at the moment are:

1. Doped RE1111 (RE=La,Ce,Pr,Nd,Sm,Tb,Dy) Fe pnictides with  $T_c$  about 25–55 K, with chemical compositions like  $\text{RE O}_{1-x}\text{F}_x\text{FeAs}$  [1, 4, 5, 6, 7, 8, 9, 10, 11].
2. Doped A122 ( $A=\text{Ba}, \text{Sr}$ ), such as  $\text{Ba}_{1-x}\text{K}_x\text{Fe}_2\text{As}_2$  [12, 13, 14, 15] and  $T_c$  about 38 K.
3. 111 systems like  $\text{Li}_{1-x}\text{FeAs}$  with  $T_c \sim 18$  K [16, 17].
4.  $(\text{Sr}, \text{Ca}, \text{Eu})\text{FFeAs}$  [18, 19] with  $T_c \sim 36$  K [21].
5.  $\text{Sr}_4(\text{Sc}, \text{V})_2\text{O}_6\text{Fe}_2(\text{P}, \text{As})_2$  with  $T_c \sim 17$  K [22].
6.  $\text{FeSe}_x$ ,  $\text{FeSe}_{1-x}\text{Te}_x$  with  $T_c$  up to 14 K [23].
7.  $(\text{K}, \text{Cs})_x\text{Fe}_{2-y}\text{Se}_2$  and similar with  $T_c$  up to 31K [24, 25].

Among these, most recently discovered Fe chalcogenides like  $\text{K}_x\text{Fe}_2\text{Se}_2$  and  $\text{Cs}_x\text{Fe}_2\text{Se}_2$  with rather high values of superconducting transition temperature:  $T_c=31\text{K}$  [24] and  $27\text{K}$  [25] were

followed by  $T_c = 31\text{K}$  in  $(\text{Tl}, \text{K})\text{Fe}_x\text{Se}_2$  [26] and form apparently a distinct new class. These systems are isostructural to the FeAs 122 - systems [2, 3], while  $T_c$  values for these Fe chalcogenides are a bit smaller than in similar pnictides. According to most recent data, in most of the chalcogenides Fe vacancies are intrinsic, so that most general chemical composition is usually written now as  $A_x\text{Fe}_{2-y}\text{Se}_2$ . In particular, Fe vacancy ordering was discovered in  $\text{K}_{0.8}\text{Fe}_{1.6}\text{Se}_2$ , and most strikingly this system seems to be an ordered antiferromagnet (AFM) with pretty large Neel temperature (about 578K) [27, 28]. Further ARPES investigations of these systems produced experimental Fermi surface maps [29, 30, 31] significantly different from previously studied for Fe pnictides [2, 3]. Review of recent findings on Fe chalcogenide superconductors can be found in Ref. [32].

In this work we discuss electronic structure, densities of states (DOS) and Fermi surfaces of Fe chalcogenides, as compared to Fe pnictides. We present some estimates on the values of  $T_c$ , demonstrating that in all Fe - based superconductors there is a definite correlation between  $T_c$  and the values of DOS at the Fermi level. Also we analyze the role of Fe vacancies and AFM ordering in  $\text{K}_x\text{Fe}_{2-x/2}\text{Se}_2$  in formation of its electronic spectrum and Fermi surfaces, which are compared with available ARPES data.

\*Corresponding author.

Email address: sadovski@iep.uran.ru (M.V. Sadovskii)

## 2. Electronic structure

There are plenty of papers on LDA band structure of La111 [33, 34, 35], LaOFeP [36], RE111 series [37], BaFe<sub>2</sub>As<sub>2</sub> [38, 39, 40], LiFeAs [41, 42], (Sr,Ca)FFeAs [43, 44], Sr42622 [45]. Electronic structure of Fe(S,Se,Te) materials was discussed in Ref. [46]. LDA calculations of electronic spectrum of newly discovered (K,Cs)<sub>x</sub>Fe<sub>2</sub>Se<sub>2</sub> were described recently in [47, 48].

To illustrate the general picture of the energy spectrum of Fe pnictides and chalcogenides in the upper part of Fig. 1 we show LDA calculated total, Fe-3d and As-4p DOS (left panel) matched with the band dispersions (right panel) for typical representatives of both classes. From Fig. 1 one can see that around the Fermi level (from -2.5 eV to +2.5 eV) there are practically only Fe-3d states present, while As-4p states are contributing at lower energies (from -2.5 eV down to -6.0 eV).

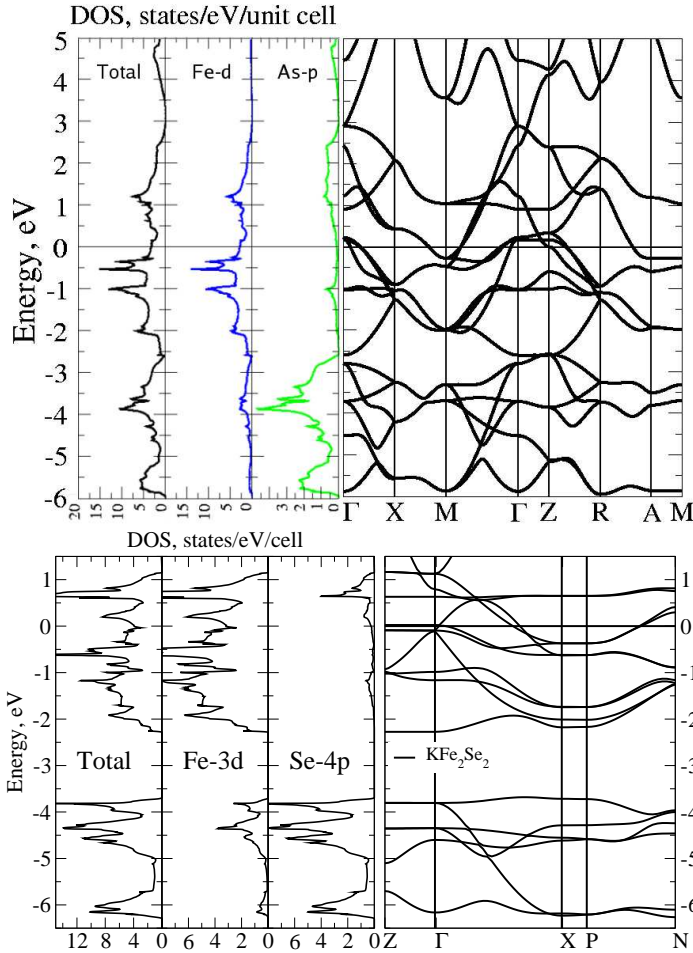


Figure 1: LDA calculated band dispersions and densities of states for typical representatives of iron based superconductors: LiFeAs (upper panel) for pnictides and KFe<sub>2</sub>Se<sub>2</sub> (lower panel) for chalcogenides. The Fermi level  $E_F$  is at zero energy.

In a bird eye (large-energy scale) view K<sub>x</sub>Fe<sub>2</sub>Se<sub>2</sub> has similar band dispersions as those in pnictides. However, there are some quantitative differences, e.g. all Fe-3d and Se-4p states in new systems are separated in energy in contrast to Fe-3d and As-4p

Ba122. Also Se-4p states are of about 0.7 eV lower than As-4p states. At the same time, similarly to pnictides the Fermi level  $E_F$  in Fe chalcogenides is crossed only by Fe-3d states.

However, at lower energy-scale there is a major difference in spectra of both classes. In Fig. 2 we compare LDA calculated electron spectrum in the immediate vicinity (relevant for superconductivity) of the Fermi level for both Ba122 [38] system and K<sub>x</sub>Fe<sub>2</sub>Se<sub>2</sub> [48]. To some extent Ba122 bands near  $E_F$  (upper part of Fig. 2) would match those for KFe<sub>2</sub>Se<sub>2</sub> if we shift them down in energy by about 0.2 eV. Main difference between old and new systems is seen around  $\Gamma$  point. For KFe<sub>2</sub>Se<sub>2</sub> systems antibonding part Se-4p<sub>z</sub> band in the Z- $\Gamma$  direction forms electron-like pocket. In Ba122 corresponding band lies about 0.4eV higher and goes much steeper, thus it is quite far away from  $\Gamma$  point. However, if we dope KFe<sub>2</sub>Se<sub>2</sub> systems (in a rigid band manner) with holes we obtain bands around  $\Gamma$  point (close to the Fermi level) very similar to those in case of Ba122. Namely at 60% hole doping we obtain Fermi surfaces with three hole-like cylinders, while stoichiometric KFe<sub>2</sub>Se<sub>2</sub> has one small electron pocket and larger hole like one near  $\Gamma$  point. Thus, in fact under hole doping we expect several topological transitions of the Fermi surfaces [48], which demonstrates potentially rich effects of doping this system.

In general, the electronic structure of new chalcogenide superconductors close to the Fermi level is significantly different from those of FeAs 122 systems. In particular no nesting of electron and hole - like Fermi surfaces is observed [48], casting doubts on some of the most popular theoretical schemes of Cooper pairing developed for iron pnictides.

## 3. Anion height and DOS control $T_c$ ?

It was discovered in Ref. [49] that superconducting temperature  $T_c$  nonmonotonically depends on anion height  $\Delta z_a$  with respect to Fe layer (see Fig. 3, triangles). Clear maximum is seen at about  $\Delta z_a \sim 1.37\text{\AA}$  (see also Table 1). Following this idea we performed systematic LDA computations of total density of states  $N(E_F)$  for number of iron based superconductors (see Fig. 3, circles and Tab. 1) which have different  $\Delta z_a$  [52]. Here we also add similar results for the new iron chalcogenides (K,Cs)Fe<sub>2</sub>Se<sub>2</sub>. Nonmonotonous behavior of DOS can be explained by hybridization effects. Namely, as a governing structural parameter characterizing hybridization strength one can chose  $a$ -Fe- $a$  angle – an angle between anions ( $a$ ) and Fe within the same tetrahedron. The value of this angle corresponding to the strongest hybridization is  $109.45^\circ$ , i.e. for an ideal anion tetrahedron with Fe in the very center of it. Other crystal structure parameters are not changed very much from system to system and do not have any transparent dependence of  $\Delta z_a$ .

To estimate superconducting critical temperature  $T_c$  as a function of the  $\Delta z_a$  one can apply the elementary BCS theory, where in the expression  $T_c = 1.14\omega_D e^{-1/\lambda}$  corresponding  $N(E_F)$  enters into the dimensionless pairing interaction constant  $\lambda = gN(E_F)/2$  ( $g$  is the appropriate dimensional coupling constant). Taking the Debye frequency  $\omega_D = 350$  K in rough accord with neutron scattering experiments on phonon density of states for La111 [50] and Ba122 [51] systems, we can find  $g$

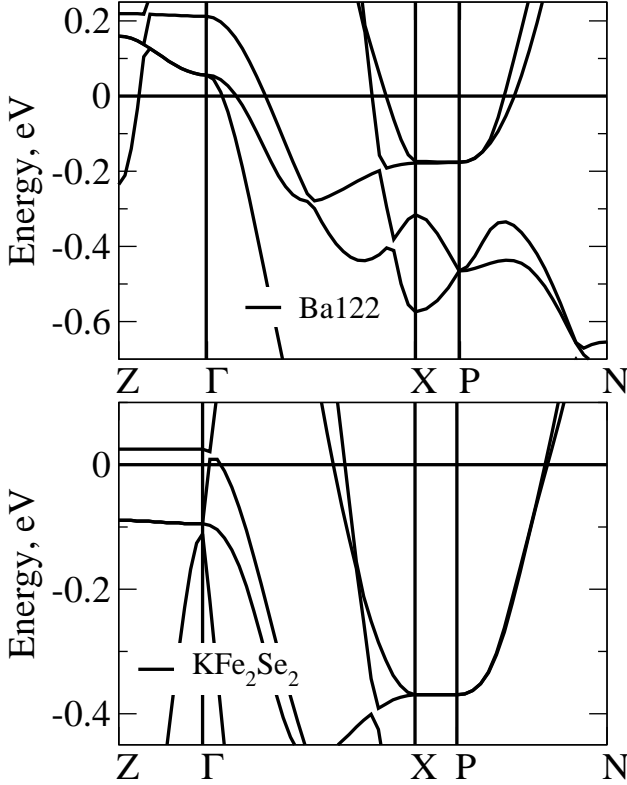


Figure 2: Top panel – LDA calculated band dispersions in the vicinity of the Fermi level for Ba122; Bottom panel – KFe<sub>2</sub>Se<sub>2</sub>. The Fermi level is at zero energy.

to fit the experimental value of  $T_c$  for Ba122 system since this system possesses probably most stable value of  $T_c$  (about 38 K) with respect to the way of sample preparation and doping. Thus we obtain the value of dimensionless coupling constant  $\lambda=0.43$ . Then just fixing the value of  $g$  as for Ba122 we obtain  $T_c$  values for all other systems, taking into account only the appropriate change of the density of states (Fig. 3, diamonds and Table 1). The agreement of these elementary estimates with experimental values of  $T_c$  is rather striking.

In fact we do not adhere at the moment to any specific pairing mechanism, as  $\omega_D$  in BCS expression does not necessarily correspond to phonon frequency, it can denote the characteristic frequency of any kind of Bosons responsible for the pairing “glue”. Our results only show unambiguous correlation between the values of superconducting  $T_c$  and those of the total density of electronic states at the Fermi level for the whole class of iron based superconductors (including the new chalcogenides), thus supporting the usual BCS-like pairing mechanism in these systems. The fit using more elaborate expression for  $T_c$ , like e.g. Allen-Dynes formula, also produces rather satisfactory results [52]. Relatively high values of effective pairing couplings, necessary to obtain experimentally observed values of  $T_c$ , can be understood as due to multiple band electronic structure of new superconductors and importance of inter - band couplings [53]. Special properties of electronic spectrum, such as widely popular “nesting” of electron and hole Fermi surfaces are not necessary at all. At the same time, inter - band *repul-*

Table 1: LDA total DOS  $N(E_F)$ , calculated and experimental  $T_c$  for iron based superconductors.

| System  | $\Delta z_a$ , Å | $N(E_F)$ , states/cell/eV | $T_c^{BCS}$ , K | $T_c^{exp}$ , K |
|---|------------------|---------------------------|-----------------|-----------------|
| LaOFeP  | 1.130            | 2.28                      | 3.2             | 6.6             |
| Sr <sub>4</sub> Sc <sub>2</sub> O <sub>6</sub> Fe <sub>2</sub> P <sub>2</sub> | 1.200            | 3.24                      | 19              | 17              |
| LaOFeAs   | 1.320            | 4.13                      | 36              | 28              |
| SmOFeAs   | 1.354            | 4.96                      | 54              | 54              |
| CeOFeAs   | 1.351            | 4.66                      | 48              | 41              |
| NdOFeAs   | 1.367            | 4.78                      | 50              | 53              |
| TbOFeAs   | 1.373            | 4.85                      | 52              | 54              |
| SrFFeAs   | 1.370            | 4.26                      | 38              | 36              |
| BaFe <sub>2</sub> As <sub>2</sub>   | 1.371            | 4.22                      | 38              | 38              |
| CaFFeAs   | 1.420            | 4.04                      | 34              | 36              |
| CsFe <sub>2</sub> Se <sub>2</sub>   | 1.435            | 3.6                       | 29              | 27              |
| KFe <sub>2</sub> Se <sub>2</sub>  | 1.45             | 3.94                      | 34              | 31              |
| LiFeAs  | 1.505            | 3.86                      | 31              | 18              |
| FeSe  | 1.650            | 2.02                      | 3               | 14              |

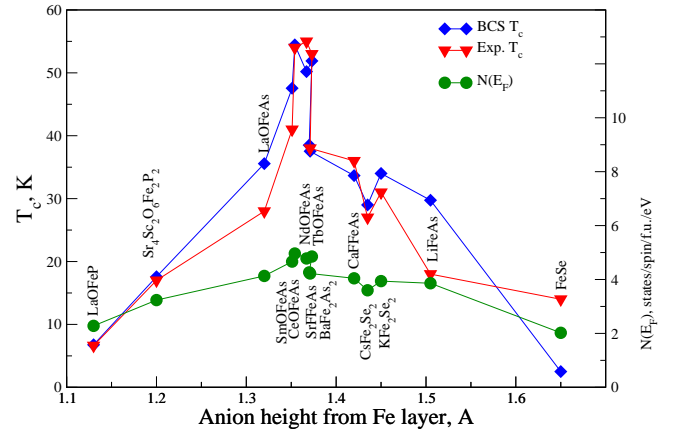


Figure 3: LDA calculated total DOS values  $N(E_F)$  (circles, right scale) and superconducting transition temperatures  $T_c$  (left scale) obtained from simple BCS (stars) and experimental  $T_c$  values (triangles) versus anion height  $\Delta z_a$  over Fe layer for a number of iron based high temperature superconductors.

sion of any kind, leading to  $s^\pm$  - pairing seems preferable (non-phonon) mechanism of pairing, facilitating higher values of  $T_c$  in both pnictides and chalcogenides.

#### 4. Vacancies and antiferromagnetism in KFe<sub>2</sub>Se<sub>2</sub>

The recent discovery [27, 28] of Fe vacancies ordering and antiferromagnetic ordering at pretty high temperature  $T_N \sim 580$  K, much exceeding superconducting  $T_c$ , in the  $A_x\text{Fe}_{2-x/2}\text{Se}_2$  ( $A=\text{K}, \text{Cs}, \text{Ti}, \dots$ ) makes these systems unique antiferromagnetic superconductors with highest  $T_N$  observed up to now. This poses some difficult problems for theoretical understanding of superconductivity. Here we discuss the role of both vacancies and AFM ordering in transformation of band structure and Fermi surfaces.

Ordering of Fe vacancies in the  $\text{K}_{0.8}\text{Fe}_{1.6}\text{Se}_2$  system [28] provides  $\sqrt{5} \times \sqrt{5}$  supercell. Corresponding ordered vacancies together with antiferromagnetic order within the Fe-layer [28]

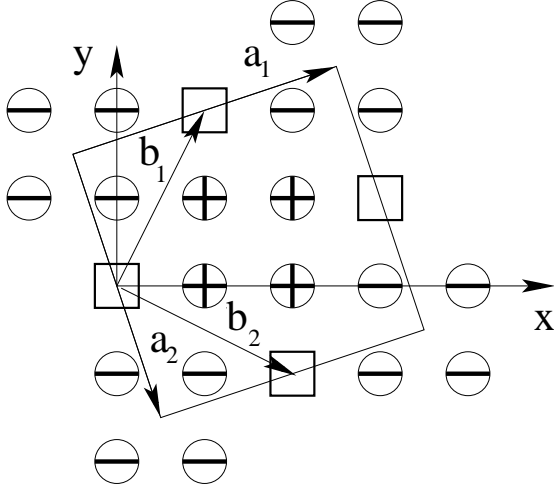


Figure 4: Schematic picture of  $K_{0.8}Fe_{1.6}Se_2$  Fe-layer with vacancies (rectangle) and experimentally observed AFM order (spin up – circles with “+” inside, spin down – circles with “-” inside). Translation vectors corresponding to AFM order are  $\mathbf{a}_1$  and  $\mathbf{a}_2$ . Translation vectors for supercell with ordered vacancies are  $\mathbf{b}_1$  and  $\mathbf{b}_2$ .

are presented in Fig. 4. Translation vectors of the supercell because of AFM order are  $\mathbf{a}_1$  and  $\mathbf{a}_2$ . Translation vectors corresponding to supercell with ordered vacancies are  $\mathbf{b}_1$  and  $\mathbf{b}_2$ .

We performed LSDA calculations for a simplified crystal structure of  $K_{0.8}Fe_{1.6}Se_2$  given in Ref. [28]. Our results are similar but not identical to other LSDA calculations on this system [54, 55]. For example we obtain metallic AFM state with finite density of states at the Fermi level, while energy gap forms at lower energies. Because of folding effects automatically included in LSDA code, it is rather difficult to make direct comparison of LSDA band structure for  $K_{0.8}Fe_{1.6}Se_2$  and its Fermi surfaces with unfolded LDA bands and Fermi surfaces like those shown above. Also Fermi surface maps from ARPES experiments [29, 30, 31] are routinely shown in the unfolded Brillouin zone of parent  $KFe_2Se_2$ , like that relevant for nonmagnetic LDA [47, 48]. So these Fermi surfaces are quite difficult to compare with extremely folded LSDA ones [54, 55].

To overcome this problem we use simplified (semi)analytic model approach first used by us in Ref. [56]. To this end we fit LDA bands of Ref. [48] with simple parabolic bare spectra in the vicinity of the Fermi level using the approach of Ref. [56] and analyze multiple electron scattering (within iron plane) by vacancies (CDW) with potential  $V_1(\mathbf{r}) = 2\Delta_1(\cos \mathbf{Q}_1\mathbf{r} + \cos \mathbf{Q}_2\mathbf{r})$  and AFM (SDW) potential  $V_2(\mathbf{r}) = 2\Delta_2(\cos \mathbf{X}_1\mathbf{r} + \cos \mathbf{X}_2\mathbf{r})$ . Corresponding vacancy CDW and SDW vectors are  $\mathbf{Q}_1 = 2\pi(0.4, 0.2)$ ,  $\mathbf{Q}_2 = 2\pi(-0.2, 0.4)$ ,  $\mathbf{X}_1 = 2\pi(0.1, 0.3)$ ,  $\mathbf{X}_2 = 2\pi(-0.3, 0.1)$ .

Initial (retarded) bare Green function is taken as:

$$g^{ij}(\mathbf{k}) = g^i \delta_{ij} = \frac{1}{E - \epsilon_i(\mathbf{k}) + i\delta} \delta_{ij} \quad (1)$$

where  $i, j$  are band indices,  $\epsilon_i(\mathbf{k})$  –  $i$ -th band model electronic spectrum. Because of multiple scattering on vacancies (CDW) and AFM (SDW) order, band electron with momentum  $\mathbf{k}$  could be scattered by any of ten possible momenta (See Table 2 of

Table 2: Table of scattering vectors summation.

|                      |                      |                |                      |                      |
|----------------------|----------------------|----------------|----------------------|----------------------|
|                      | $\mathbf{Q}_1$       | $\mathbf{Q}_2$ | $\mathbf{Q}_1$       | $\mathbf{Q}_2$       |
| $\mathbf{Q}_1$       | $\mathbf{Q}_2$       | $\mathbf{Q}_2$ | 0                    | $\bar{\mathbf{Q}}_1$ |
| $\mathbf{Q}_2$       | $\mathbf{Q}_2$       | $\mathbf{Q}_1$ | $\mathbf{Q}_1$       | 0                    |
| $\bar{\mathbf{Q}}_1$ | 0                    | $\mathbf{Q}_1$ | $\bar{\mathbf{Q}}_2$ | $\mathbf{Q}_2$       |
| $\mathbf{Q}_2$       | $\mathbf{Q}_1$       | 0              | $\mathbf{Q}_2$       | $\mathbf{Q}_1$       |
|                      | $\mathbf{Q}_1$       | $\mathbf{Q}_2$ | $\mathbf{Q}_1$       | $\mathbf{Q}_2$       |
| $\mathbf{X}_1$       | $\mathbf{Y}$         | $\mathbf{X}_1$ | $\mathbf{X}_2$       | $\bar{\mathbf{X}}_2$ |
| $\mathbf{X}_2$       | $\mathbf{X}_1$       | $\mathbf{Y}$   | $\mathbf{X}_2$       | $\bar{\mathbf{X}}_1$ |
| $\bar{\mathbf{X}}_1$ | $\bar{\mathbf{X}}_2$ | $\mathbf{X}_2$ | $\mathbf{Y}$         | $\mathbf{X}_1$       |
| $\bar{\mathbf{X}}_2$ | $\mathbf{X}_2$       | $\mathbf{X}_1$ | $\mathbf{X}_1$       | $\mathbf{Y}$         |

|                      |                |                |                      |                      |
|----------------------|----------------|----------------|----------------------|----------------------|
|                      | $\mathbf{X}_1$ | $\mathbf{X}_2$ | $\bar{\mathbf{X}}_1$ | $\bar{\mathbf{X}}_2$ |
| $\mathbf{X}_1$       | $\mathbf{Q}_2$ | $\mathbf{Q}_2$ | 0                    | $\mathbf{Q}_1$       |
| $\mathbf{X}_2$       | $\mathbf{Q}_2$ | $\mathbf{Q}_1$ | $\bar{\mathbf{Q}}_1$ | 0                    |
| $\bar{\mathbf{X}}_1$ | 0              | $\mathbf{Q}_1$ | $\mathbf{Q}_2$       | $\bar{\mathbf{Q}}_2$ |
| $\bar{\mathbf{X}}_2$ | $\mathbf{Q}_1$ | 0              | $\bar{\mathbf{Q}}_2$ | $\mathbf{Q}_1$       |

|                           |                |                |                      |                      |                |                |                      |                      |
|---------------------------|----------------|----------------|----------------------|----------------------|----------------|----------------|----------------------|----------------------|
|                           | $\mathbf{Q}_1$ | $\mathbf{Q}_2$ | $\bar{\mathbf{Q}}_1$ | $\bar{\mathbf{Q}}_2$ | $\mathbf{X}_1$ | $\mathbf{X}_2$ | $\bar{\mathbf{X}}_1$ | $\bar{\mathbf{X}}_2$ |
| $\mathbf{Y} = (\pi, \pi)$ | $\mathbf{X}_1$ | $\mathbf{X}_2$ | $\mathbf{X}_1$       | $\mathbf{X}_2$       | $\mathbf{Q}_1$ | $\mathbf{Q}_2$ | $\mathbf{Q}_1$       | $\mathbf{Q}_2$       |

scattering vectors summation). Namely, electron can preserve its momentum, or change it in nine other ways, being scattered by  $\mathbf{Q}_l$ ;  $\bar{\mathbf{Q}}_l = -\mathbf{Q}_l$  ( $l = 1, 2$ );  $\mathbf{X}_l$ ;  $\bar{\mathbf{X}}_l = -\mathbf{X}_l$  ( $l = 1, 2$ );  $\mathbf{Y} = (\pi, \pi)$ . Thus, to find one-band diagonal Green’s function  $G(\mathbf{k}, \mathbf{k}) \equiv G$  and nine off-diagonal:  $G(\mathbf{k} \pm \mathbf{Q}_l, \mathbf{k}) \equiv F_{l(\bar{l})}$ ,  $G(\mathbf{k} \pm \mathbf{X}_l, \mathbf{k}) \equiv \Phi_{l(\bar{l})}$  and  $G(\mathbf{k} \pm \mathbf{Y}, \mathbf{k}) \equiv \Psi$ , we end up with system of 10 linear equations. Such approach can also be generalized to the multiple band case in a simplified way similar to that used in Ref. [56], assuming that for both vacancy and SDW scattering both inter- and intraband scattering amplitudes are identical. Thus we can obtain for the multiple case the system of ten linear equations for following Green functions –  $G^{ij}$ ,  $F_{l(\bar{l})}^{ij}$ ,  $\Phi_{l(\bar{l})}^{ij}$ ,  $\Psi^{ij}$ , which now have two band indices. The equation for diagonal Green function is written as:

$$G^{ij} = g^i \delta_{ij} + g^i \sum_{l=1\bar{2}\bar{1}\bar{2}} [\Delta_1 \sum_m F_l^{mj} + \Delta_2 \sum_m \Phi_l^{mj}]. \quad (2)$$

Once we sum up over  $i$  we come to

$$G^j = g^j + g \sum_{l=1\bar{2}\bar{1}\bar{2}} [\Delta_1 F_l^j + \Delta_2 \Phi_l^j]. \quad (3)$$

The rest of other nine equations for  $G^j = \sum_i G^{ij}$ ,  $F_l^j = \sum_i F_l^{ij}$ ,  $\Phi_l^j = \sum_i \Phi_l^{ij}$ ,  $\Psi^j = \sum_i \Psi^{ij}$  can be obtained using Table 2 of scattering vectors summation. More details on this approach will be presented in Ref. [57], devoted to similar model of hexagonal transition metal dichalcogenides, like  $NbSe_2$  and  $TaSe_2$ .

Finally by solving this system of linear equations we can get the diagonal Green’s function  $G^{ij}(\mathbf{k}, \mathbf{k})$  ( $i, j$  – band indices) and define spectral functions

$$A(E, \mathbf{k}) = -\frac{1}{\pi} \text{Im} \sum_i G^{ii}(\mathbf{k}, \mathbf{k}). \quad (4)$$

To account for finite experimental spectral resolution we broaden all our results by substituting  $E \rightarrow E + i\gamma$ , with  $\gamma = 0.03\text{eV}$ , corresponding to typical ARPES resolution.

The values of model scattering amplitudes  $\Delta_1$  and  $\Delta_2$  and chemical potential were obtained by approximate fitting DOS obtained from our model calculations (solid line in Fig. 5) to

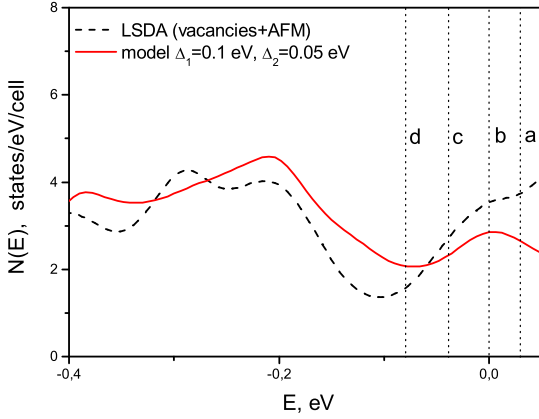


Figure 5: Comparison of part of total LSDA DOS (dashed line) for  $K_xFe_{2-x/2}Se_2$  with model DOS (solid line) obtained from parabolic bare bands with vacancy (CDW) and AFM (SDW) scattering taken into account. Fermi level is zero. Letters a,b,c and d denote different doping levels, corresponding to different Fermi surfaces shown in Fig. 7.

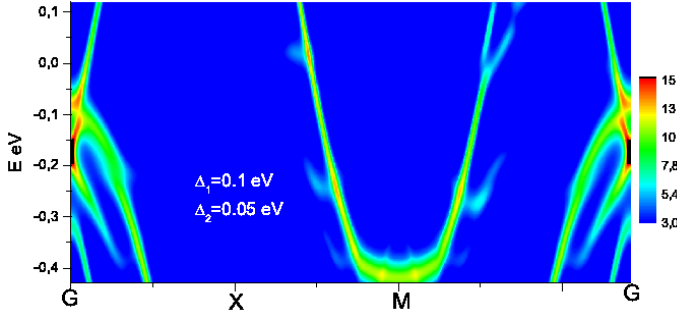


Figure 6: Model spectral function map for  $K_xFe_{2-x/2}Se_2$  obtained from parabolic bare bands with vacancy (CDW) and AFM (SDW) scattering taken into account. Fermi level is zero.

(similarly broadened) LSDA DOS (dashed line in Fig. 5) in a narrow energy interval close to the Fermi level. It can be seen that this fit is rather good in this energy interval, where parabolic (two-dimensional) fit for energy bands is also satisfactory.

In Fig. 6 model spectral function map (4) for  $K_xFe_{2-x/2}Se_2$  is presented. As mentioned above the bare spectra in the vicinity of the Fermi level were modelled by a number of parabolas (cf. Ref. [56]). The general broadening (finite life time effects) comes out from finite  $\gamma$  resolution effects. Quasiparticle bands with additional shadow like features due to vacancy and AFM ordering are clearly seen and can be observed in ARPES experiments. These bands are to be compared with simple LDA results of Ref. [48], shown in the lower part of Fig. 2.

Model Fermi surface maps for  $K_xFe_{2-x/2}Se_2$  with vacancies and AFM (SDW) taken into account for different doping levels are shown in Fig. 7. Panel (a) of Fig. 7 corresponds to electron doped case, panel (b) – undoped and panels (c) and (d) – hole

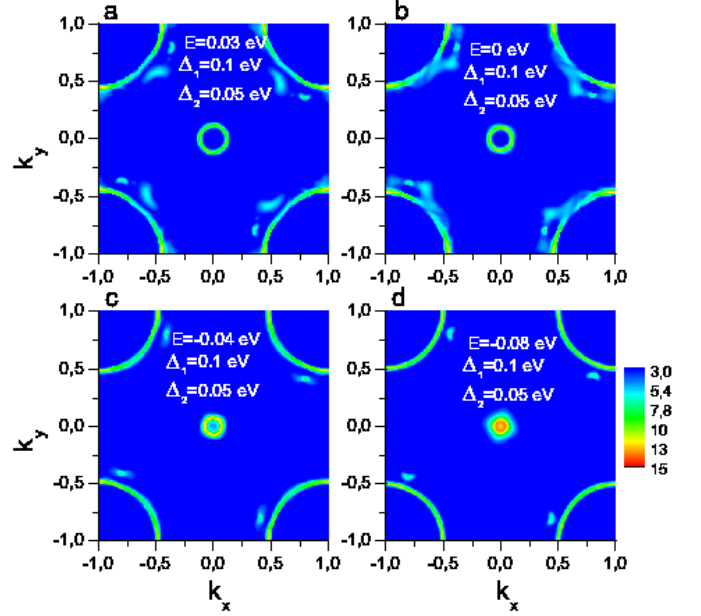


Figure 7: Model Fermi surface maps for  $K_xFe_{2-x/2}Se_2$  obtained from parabolic bare bands with vacancy (CDW) and AFM (SDW) scattering taken into account. Panels a,b,c and d correspond to doping levels shown on Fig. 5.

doped case. Corresponding doping levels are displayed also on Fig. 5. These (model) theoretical results are very similar to experimental data of Refs. [29, 30, 31], with rather large (electronic) cylinders around  $(\pi, \pi)$ -point and rather small or even almost completely smeared out cylinders around  $\Gamma$ -point were observed. Similar picture was found also for parent  $KFe_2Se_2$  system in simple LDA [48]. Presence of vacancy (CDW) and AFM (SDW) scattering leads only to formation of some low intensive shadow Fermi surfaces which would be rather hard to detect in ARPES experiments. In fact, most ARPES investigations of these system demonstrate experimental Fermi surface maps quite similar to those shown in Fig. 7 [29, 30, 31].

The most important conclusion is that, rather unexpectedly, the role of vacancy scattering and antiferromagnetic ordering in the formation of electronic spectrum in the vicinity of the Fermi level is rather minor. The system remains metallic with well defined Fermi surfaces, allowing the formation of superconducting state on the background of AFM and vacancy order [58].

## 5. Conclusion

In this work we present comparative study of iron based pnictide and chalcogenide superconductors. It was shown that for both families superconducting transition temperature is apparently controlled by anion height  $\Delta z_a$  with respect to Fe plane, which is directly correlated with the values of DOS at the Fermi level. Unfolded Fermi surfaces observed in the ARPES experiments even in strong antiferromagnet  $K_{0.8}Fe_{1.6}Se_2$  with ordered

Fe vacancies are very similar to those of parent (nonmagnetic)  $\text{KFe}_2\text{Se}_2$ . The system remains metallic despite AFM and vacancy ordering and superconducting state with rather high  $T_c$  forms on this unusual background.

## 6. Acknowledgements

This work is partly supported by RFBR grant 11-02-00147 and was performed within the framework of programs of fundamental research of the Russian Academy of Sciences (RAS) “Quantum physics of condensed matter” (09-II-2-1009) and of the Physics Division of RAS “Strongly correlated electrons in solid states” (09-T-2-1011).

## References

- [1] Y. Kamihara, T. Watanabe, M. Hirano, H. Hosono. *J. Am. Chem. Soc.* **130**, 3296-3297 (2008).
- [2] M.V. Sadovskii, *Uspekhi Fiz. Nauk* **178**, 1243 (2008); *Physics Uspekhi* **51**, No. 12 (2008); arXiv: 0812.0302.
- [3] K. Ishida, Y. Nakai, H. Hosono. *J. Phys. Soc. Jpn.* **78**, 062001 (2009).
- [4] G.F. Chen, Z. Li, G. Zhou, D. Wu, J. Dong, W.Z. Hu, P. Zheng, Z.J. Chen, J.L. Luo, N.L. Wang, *Phys. Rev. Lett.* **101**, 057007 (2008).
- [5] X. Zhu, H. Yang, L. Fang, G. Mu, H.-H. Wen. *Supercond. Sci. Technol.* **21**, 105001 (2008).
- [6] A.S. Sefat, M.A. McGuire, B.C. Sales, R. Jin, J.Y. Hove. D. Mandrus, *Phys. Rev. B* **77**, 174503 (2008).
- [7] G. F. Chen, Z. Li, D. Wu, G. Li, W. Z. Hu, J. Dong, P. Zheng, J. L. Luo, N. L. Wang, *Phys. Rev. Lett.* **100**, 247002 (2008).
- [8] X. H. Chen, T. Wu, G. Wu, R. H. Liu, H. Chen, D. F. Fang. *Nature* **453**, 761 (2008).
- [9] Z.-A. Ren, J. Yang, W. Lu, W. Yi, X.-L. Shen, G.-C. Che, L.-L. Sun, F. Zhou, Z.-X. Zhao. *Europhys. Lett.* **82**, 57002 (2008).
- [10] Z.-A. Ren, J. Yang, W. Lu, W. Yi, G.-C. Che, X.-Li. Dong, L.-L. Sun, Z.-X. Zhao. *Materials Research Innovations* **12**, 105 (2008).
- [11] J.-W. G. Bos, G. B. S. Penny, J. A. Rodgers, D. A. Sokolov, A. D. Huxley and J. P. Attfield, *Chem. Commun.* **31**, 3634 (2008).
- [12] M. Rotter, M. Tegel, D. Johrendt. *Phys. Rev. Lett.* **101**, 107006 (2008).
- [13] G.F. Chen, Z. Li, G. Li, W.Z. Hu, J. Dong, X.D. Zhang, N.L. Wang, J.L. Luo. *Chin. Phys. Lett.* **25**, 3403 (2008).
- [14] K. Sasmal, B. Lv, B. Lorenz, A. Guloy, F. Chen, Y. Xue, C.W. Chu. *Phys. Rev. Lett.* **101**, 107007 (2008).
- [15] N. Ni, S.L. Bud'ko, A. Kreyssig, S. Nandi, G.E. Rustan, A.I. Goldman, S. Gupta, J.D. Corbett, A. Kracher, P.C. Canfield. *Phys. Rev. B* **78**, 014507 (2008).
- [16] J.H. Tapp, Z. Tang, Bing Lv, K. Sasmal, B. Lorenz, Paul C.W. Chu, A. M. Guloy. *Phys. Rev. B* **78**, 060505(R) (2008).
- [17] X.C. Wang, Q.Q. Liu, Y.X. Lv, W.B. Gao, L.X. Yang, R.C. Yu, F.Y. Li, C.Q. Jin, *Solid State Commun.* **11-12**, 538 (2008).
- [18] M. Tegel, S. Johansson, V. Weiss, I. Schellenberg, W. Hermes, R. Poettgen, D. Johrendt, *Europhys. Lett.* **84**, 67007 (2008).
- [19] F. Han, X. Zhu, G. Mu, P. Cheng, H.H. Wen, *Phys. Rev. B* **78**, 180503 (2008).
- [20] S. Matsuishi, Y. Inoue, T. Nomura, M. Hirano, H. Hosono. *J. Phys. Soc. Jpn.* **77**, 113709 (2008); *J. Am. Chem. Soc.* **130**, 14428 (2008).
- [21] X. Zhu, F. Han, P. Cheng, G. Mu, B. Shen, Hai-Hu Wen, *Europhys. Lett.* **85**, 17011 (2009).
- [22] H. Ogino, Y. Katsura, S. Horii, K. Kishio, J. Shimoyama, *Supercond. Sci. Technol.* **22** (2009); Y.L. Xie, R.H. Liu, T. Wu, G. Wu, Y.A. Song, D. Tan, X.F. Wang, H. Chen, J.J. Ying, Y.J. Yan, Q.J. Li, X.H. Chen, *Euro. Phys. Lett.* **86**, 57007 (2009); G.F. Chen, T.L. Xia, P. Zheng, J.L. Luo, N.L. Wang, *Supercond. Sci. Technol.* **22** (2009).
- [23] F. C. Hsu, J. Y. Luo, K. W. Yeh, T. K. Chen, T. W. Huang, P. M. Wu, Y. C. Lee, Y. L. Huang, Y. Y. Chu, D. C. Yan, and M. K. Wu, *Proceedings of the National Academy of Sciences*, 2008, volume 105, 14262.
- [24] J. Guo, S. Jin, G. Wang, S. Wang, K. Zhu, T. Zhou, M. He, and X. Chen, *Phys. Rev. B* **82**, 180520(R) (2010).
- [25] A. Krzton-Maziopa, Z. Shermadini, E. Pomjakushina, V. Pomjakushin, M. Bendele, A. Amato, R. Khasanov, H. Luetkens, K. Conder, arXiv:1012.3637v1.
- [26] M. Fang, H. Wang, C. Dong, Z. Li, C. Feng, J. Chen, H.Q. Yuan, arXiv:1012.5188
- [27] Z. Shermadini, A. Krzton-Maziopa, M. Bendele, R. Khasanov, H. Luetkens, K. Conder, E. Pomjakushina, S. Weyeneth, V. Pomjakushin, O. Bossen, and A. Amato, *Phys. Rev. Lett.* **106**, 117602 (2011).
- [28] W. Bao, Q. Huang, G. F. Chen, M. A. Green, D. M. Wang, J. B. He, X. Q. Wang, Y. Qiu, arXiv:1102.0830v1.
- [29] D. Mou *et. al*, *Phys. Rev. Lett.* **106**, 107001 (2011).
- [30] X.-P. Wang, T. Qian, P. Richard, P. Zhang, J. Dong, H.-D. Wang, C.-H. Dong, M.-H. Fang, H. Ding, *Europhysics Letters* **93**, 57001 (2011).
- [31] L. Zhao *et. al*, *Phys. Rev. B* **83**, 140508(R) (2011).
- [32] A.L. Ivanovskii, arXiv:1104.3400
- [33] D.J. Singh, M.H. Du. *Phys. Rev. Lett.* **100**, 237003 (2008).
- [34] L. Boeri, O.V. Dolgov, A.A. Golubov, *Phys. Rev. Lett.* **101**, 026403 (2008).
- [35] I.I. Mazin, D.J. Singh, M.D. Johannes, M.H. Du, *Phys. Rev. Lett.* **101**, 057003 (2008).
- [36] S. Lebegue, *Phys. Rev. B* **75**, 035110 (2007).
- [37] I.A. Nekrasov, Z.V. Pchelkina, M.V. Sadovskii. *JETP Letters* **87**, 560 (2008).
- [38] I.A. Nekrasov, Z.V. Pchelkina, M.V. Sadovskii. *JETP Letters*, **88**, 144 (2008).
- [39] I.R. Shein, A.L. Ivanovskii, *JETP Letters*, **88**, 107 (2008).
- [40] C. Krellner, N. Caroca-Canales, A. Jesche, H. Rosner, A. Ormeci, C. Geibel, *Phys. Rev. B* **78**, 100504(R) (2008).
- [41] I.A. Nekrasov, Z.V. Pchelkina, M.V. Sadovskii. *JETP Letters* **88**, 543 (2008).
- [42] I.R. Shein, A.L. Ivanovskii, *JETP Letters*, **88**, 329 (2008).
- [43] I.A. Nekrasov, Z.V. Pchelkina, M.V. Sadovskii. *JETP Letters* **88**, 679 (2008).
- [44] I.R. Shein, A.L. Ivanovskii, *JETP Letters*, **88**, 683 (2008).
- [45] I.R. Shein, A.L. Ivanovskii, *Phys. Rev. B* **79**, 245115 (2009); *J Supercond Nov Magn (Lett.)* **22** 613 (2009).
- [46] A. Subedi, L. Zhang, D. J. Singh, and M. H. Du. *Phys. Rev. B* **78**, 134514 (2008).
- [47] I.R. Shein, A.L. Ivanovskii, *Physics Letters A* **375**, 1028 (2011).
- [48] I.A. Nekrasov, M.V. Sadovskii, *JETP Letters*, **93**, 166 (2011).
- [49] Y. Mizuguchi, Y. Hara, K. Deguchi, S. Tsuda, T. Yamaguchi, K. Takeda, H. Kotegawa, H. Tou and Y. Takano, *Supercond. Sci. Technol.* **23**, 054013 (2010).
- [50] A.D. Christianson, M.D. Lumsden, O. Delaire, M.B. Stone, D.L. Abernathy, M.A. McGuire, A.S. Sefat, R. Jin, B.C. Sales, D. Mandrus, E.D. Mun, P.C. Canfield, J.Y.Y. Lin, M. Lucas, M. Kresh, J.B. Keith, B. Fultz, E.A. Goremychkin, R.J. McQueeney, *Phys. Rev. Lett.* **101**, 157004 (2008).
- [51] R. Mittal, Y. Su, S. Sols, T. Chatterji, S.L. Chaplot, H. Schober, M. Rotter, D. Johrendt, Th. Brueckel. *Phys. Rev. B* **78**, 104514 (2008).
- [52] E.Z. Kuchinskii, I.A. Nekrasov, M.V. Sadovskii, *JETP Letters*, **91**, 518 (2010).
- [53] E.Z. Kuchinskii, M.V. Sadovskii, *JETP Letters*, **89**, 156 (2009); *Physica C* **470**, S418 (2010).
- [54] C. Cao, J. Dai, arXiv:1102.1344.
- [55] X.-W. Yan, M. Gao, Z.-Y. Lu, T. Xiang, arXiv:1102.2215.
- [56] E.Z. Kuchinskii, M.V. Sadovskii, *JETP Lett.* **91**, 661 (2010).
- [57] E.Z. Kuchinskii, I.A. Nekrasov, M.V. Sadovskii (in preparation)
- [58] L.N. Bulaeviskii, A.I. Buzdin. *Sov. Phys. - Uspekhi* **29**, 412 (1986)